INTERNATIONAL JOURNAL OF
ENERGY AND ENVIRONMENT

Volume 9, Issue 3, 2018 pp.211-232
Journal homepage: www.IJEE.IEEFoundation.org

Investigation on heat transfer augmentation using continuous and broken ribs on a plate of heat exchanger

Ghassan Fadhil Smaisim

Mechanical Engineering Department, University of Kufa, Iraq.

Received 29 Nov. 2017; Received in revised form 18 Jan. 2018; Accepted 23 Jan. 2018; Available online 1 May 2018

Abstract
Experimental and theoretical studies of the force convection heat transfer throughout a rectangular channel have been obtained. Rectangular rib surfaces inserted to improve the heat transfer amount from the heated plate to the working fluid with inlet velocity that achieves Reynolds numbers between the 500 and 2000 to cover a large range of laminar flow. Different parameters of the rectangular ribs (number of continuous ribs, number of discrete of rib, row arrangement) have been explored. In experimental work, the channel length to hydraulic diameter (L/D_h) is 3, an aspect ratio W/H of 2, roughness pitch p/e of 10, roughness height e/D_h of 0.06, and the attack angle of 90^o. Nusselt numbers and the friction factor parameters compared with the corresponding values of the smooth channel at similar condition. The local heat coefficients and local hydrodynamic parameters have been obtained using the commercial ANSYS CFX 14.0 package. Numerical analysis extended to calculate the Nusselt number at $6.66 \leq p/e \leq 15$, $0.064 \leq e/H \leq 0.096$, $0.048 \leq e/D_h \leq 0.072$. Comparisons of the heat results, the pressure drop and the thermal performance via earlier results have been collected. It's observed that Nusselt number increases with Reynolds number and with use the rib surface for all models. The maximum enhancement in Nusselt number ratio observed to be 2.17 times the value of smooth channel for model 7 and friction factor is observed to be 2.18 for model 3. The overall enhancement ratio was 1.68-1.736 at Reynolds number about 1500 and its value declare slightly as the friction factor increases at the range near the transition regime. The best type of models was number 7. Heat transfer enhanced by rising the roughness height at fixed relative roughness pitch or by reducing the roughness pitch at fixed roughness height. Roughness pitch p/e could be augmented up to 10, further that there is a reduce in the heat transfer enhancement. The results compared with previous works and give good agreements.

Keywords: Augmentation heat transfer; Plate heat exchanger; Vortex generator; CFD.

1. Introduction
Heat transfer augmentation is the technique of improving the overall performance of the heat transfer for the system with reduces the cost and sizes of the heat exchangers especially for the laminar regime, as the heat transfer coefficients are in general low. During recent years, many researchers attempt to apply different active and passive mechanisms for heat transfer enlargement in compact types of the heat exchangers for the automotive industry, internal cooling for gas turbine blades, nuclear reactors, air conditioning, refrigerant applications, electrical circuits in electronic chipsets, compact heat exchangers

etc [1]. Heat transfer can be improved by inserting different types of turbulators like surface ribs by [2-4], dimples by [5-7] twisted tapes by [8-10], types of pin fins by [11-13] in additional to other the types of the vortex generators [14-20] that used to develop heat transfer rates in channels.

Installing ribs to a coolant duct are widely used to enhance heat transfer between fluid flow and solid surfaces as it causes a flow separation and reattachment to break the laminar sublayer. The rib augments the heat transfer by separate the flow, both in front and behind a rib, making of large vortex formations and the heat transfer improved by produce the secondary flow structures. Karwa et. al [2] reported that 10-40% enhanced thermal efficiency was gained by inserting ribs on the plates of air heaters. Many studies have been performed to discover the optimal conditions of various parameters for the rib design include rib arrangement, rib height, rib-to-rib pitch and angle of attack. A good review [21-24] have been presented for the works that dealing with different shapes of vortex generators, arrangement, dimension, shape of pipe and channel, number of vortex generators, angle of attack which produced to increase the heat transfer. The review showed the ribs have good effects on the thermal performance and friction factor. Heat transfer enhancement ratio in ribbed channels changed between 2.0 to 3.5 times the values that mentioned early by Dittus and Boelter [25], this is because of the modified of the modern shapes of the vortex generators nowadays which produce more efficient of the system [23]. For rib-roughened surfaces, the thermal performance impaired by increasing Reynolds number or declining channel height-to-width (H/W) ratio [4]. The pressure drops for the rectangular channel with H/W ratio of 0.25 are about 8–16 times of the square channel for the same heat transfer enhancement ratio is to be realized [3].

Han [26] studied the effect of the square ribbed channel with e/D_h=0.063 on the amount of heat transfer enhancement with relative roughness ratio (pitch ratio) p/e=10. They showed that the amount of the fluid flow had an important effect on the heat transfer coefficient beside the height of the rib that present a turbulence effect and causes an increase in the heat transfer from the hot surfaces. Prasad and Saini [27] investigated the effects of the protrusion wires and rectangular ribs on the amount of the heat transfer augmentation through the flat plate for flow regime in fully developed. They tested pitch ratio (p/e) of 0.75, 1.25, 2, 5, 8, 10 and 12 with blockage ratio (e/H) of 1,2,3,4 and 5. They concluded that the enhancement in Nusselt number was 10.69% with an increase of friction factor about 6.2%. They concluded also that the reattachment of shear layer did not happen until p/e=8 since of the flow will separate downstream and the enhancement will increase by reducing the pitch ratio for the same height ratio and the best value of the enhancement was at p/e=10.

Maa et al [28] investigated the influence of rib height and inlet temperature on the heat transfer performances of the ribbed channel. The temperature of the inlet air changed from 577^{o}C to 977^{o}C and the roughness height ratio e/H was changed from 0.083 to 0.333. They showed that the height of the rib helps to disturb the fluid flow through the channel and increase the thermal action beside the effect of the inlet velocity on the amount of the heat transfer. They also concluded that the change of the temperature of the inlet air did not influence on the fluid profile.

Whereas Fouladi [29] investigated experimentally the enhancement of heat transfer using a square rib fitted on a plate through a close loop tunnel using X probe hotwire anemometer to record the turbulence of the flow over 10mm rib height with Reynolds number range from 1300 to 6300. They concluded that the ribbed plate produced an augmentation of heat transfer for all values of inlet velocity besides a decreasing in the overall enhancement from the 1300 to 2600 as the changeover of the boundary layer occurs and the flow regime is turbulent flow. Yang et al [30] investigated experimentally a square channel with staggered and inline ribs arrangement on the overall heat transfer augmentation with Reynolds number range from 1400 to 9000 at rib height to the channel height ratios are 0.33 and 0.2, respectively and rib spacing to height ratio were from 5 to 15. The main conclusions are The Reynolds number effect directly with the Nusselt number beside to the best heat transfer coefficient occured at p/e was 10. They concluded that the inline arrangement were more efficient than the staggered arrangement.

In the present study, and according to the conclusions of Yang et al [30], several inline arrangements of rectangular ribs in continuous and broken ribs style (single, double and triple) have been mounted on flat plate, p/e of 10, e/H of 0.08, e/D_h of 0.06 which supplied to constant heat flux (Table 1). The inlet flow rates exposed to the test section were achieved to laminar airflow with range 500 to 2000. The objective of this work is to augment the heat transfer and get the most suitable number and position of ribs by varying the geometrical parameters. The goal of these cases is estimating the maximum enhancement in heat transfer causing a minimum increase in pressure drop.

Table 1. Models dimensions of the present work.

Model no.	All dimension of the models in (mm)								
	L=500 (50 H_r)	W=250 (25 H_r)	H=125 (12.5 H_r)	a_r=25 (2.5 H_r)	H_r=e=10	b_r	X_w	X_r= p	X_{br}
1	One Rib					25 H_r	0	-	-
2	Two Ribs					25 H_r	0	10 H_r	-
3	Three Ribs					25 H_r	0	10 H_r	-
4	One Rib Parted Into Three Pieces					5 H_r	2.5 H_r	-	2.5 H_r
5	One Rib Parted Into Two Pieces					8.75 H_r	2.5 H_r	-	2.5 H_r
6	Two Ribs Parted Into Two Pieces In Inline Arrangement					8.75 H_r	2.5 H_r	10 H_r	2.5 H_r
7	Two Parted Ribs Into Three Pieces In Inline Arrangement					5 H_r	2.5 H_r	10 H_r	2.5 H_r

2. Experimental rig

Figure 1 shows a schematic diagram for the experimental apparatus that consisted of the inlet section, centrifugal blower, test section with ribs, electric heater, control system for power supply, thermocouples and pressure measurement with the pitot-static tube, using an inclined manometer.

Figure 2 shows photography of the experimental rig, the air was flowing by suction process along the duct using a blower (1.25) Kw through a nozzle and mesh to produce a uniform flow at minimum turbulence intensity in the inlet section and the air exhausted into the atmosphere. The test section has dimensions of 250mm in wide and 125mm in height with corresponding hydraulic diameter, D_h =166.6667mm, and a length of 500 mm ($3D_h$). The duct of the entire, test and exit channel were prepared of Perspex material with clear ACRYLIC plates had low thermal conductivity 0.19 W/m.K with 10 mm thickness to prevent the heat transfer to and/or from the fluid flow. The heater positioned at the bottom wall of the test section. With following the steps of Yang et al [30], the plate of the heating Aluminum is painted by black paint to assure a homogeneous emissivity of 0.95. An Aluminum sheet contains the heater, which covers from the top by epoxy and from the bottom by 15mm thickness of Bakelite slab that considered a good insulator as the thermal conductivity was 0.06W/m.K to prevent the heat transfer away and allow the heat transferred upwards and to the upper Aluminum plate, which faces the fluid flow. Ribs are fitted as motivated by Yang et al [30] with Non-Silicone heat transfer compound glue type (RS 503-357) from RS Company, which had a thermal conductivity of 2.5 W/m.K. Two devices of Thermometer temperature loggers were collect to record the temperature of 17 thermocouples of K-type (TP-01) were collected to the rig. A single thermocouple was fit at the entrance region and another one at the exit region to record the temperature of the inlet and outlet respectively and 15 thermocouples were fixed by drilling holes of (0.1cm) diameter in the bottom of the plate and enter (1.5 mm) deep to evaluate the local temperature in different positions. Thermometer Calibrator type TC-920, were used to calibrate the Thermometer temperature logger, the calibration results appear that the error percentages are practically 2.39 %. Another calibration was produced to calibrate the thermocouples in the experiment elements with an error of 1.05%. Figure 3(a) shows the comparison between thermometer calibrator and digital thermometer readings, while Figure 3(b) shows the calibration curve of thermocouples reading. A calibrated digital anemometer (Model DA40) was used to measure the air velocity and a standard Pitot - static tube was used measure the pressure drop through the channel by fixed into the ends of the channel and connected to the inclined manometer, which contains a fluid with specific density 0.79. Rotary Regavolt Variac connected to reduce the voltage source to the required value of electric power supplied to the heater.

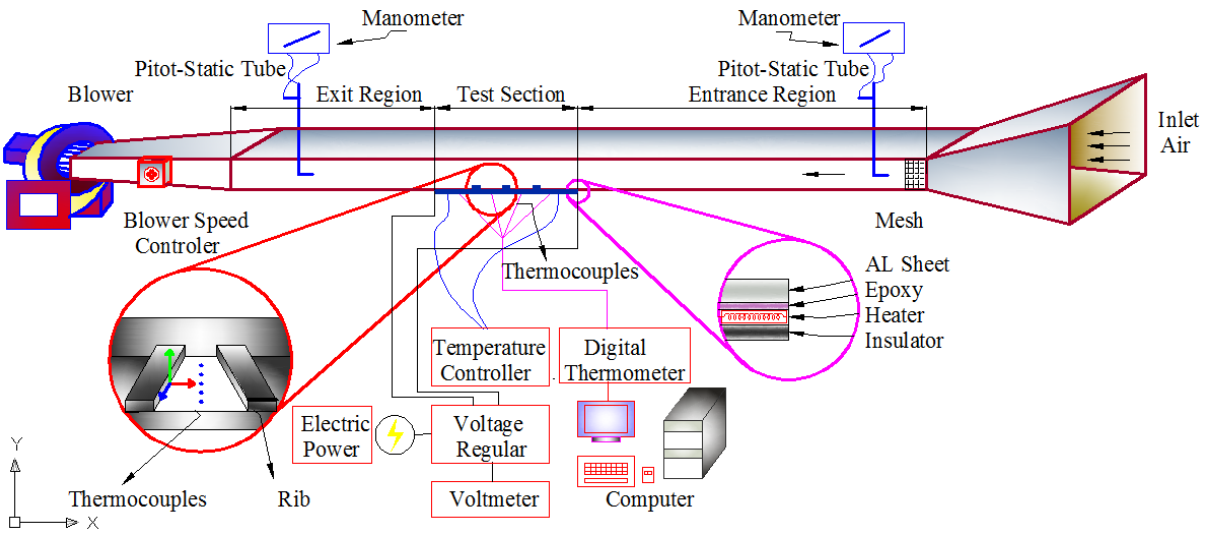

Figure 1. Schematic diagram of the experimental rig.

Figure 2. Photography of the experimental rig.

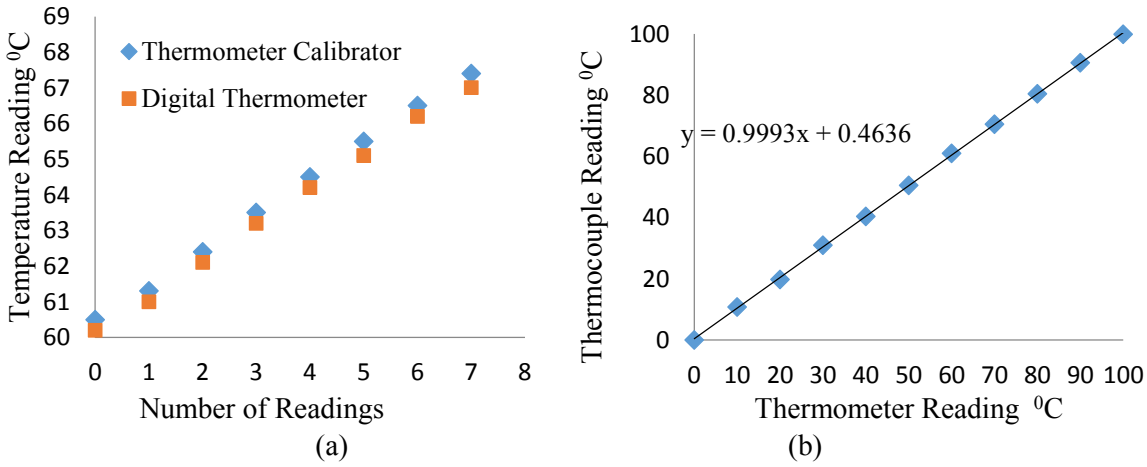

Figure 3. Calibration curves of (a) Data logger and (b) Thermocouple reading.

2.1 Data analysis method

The common steps that applied to calculate the heat transfer coefficient and Nusselt number experimentally and theoretically was produce in this section. The mean plate temperature is the average of every temperature of the thermocouples that fitted on the plate surface [1]:

$$T_{pm} = \frac{T_{p1}+T_{p2}+T_{p3}+\cdots+T_{p15}}{15} \quad (1)$$

While the bulk mean fluid temperature, is the mean of the inlet and the outlet temperatures of the fluid flows throughout the test section [1]:

$$T_{bm} = \frac{T_{in}+T_{out}}{2} \quad (2)$$

The total input power supplied to cylinder from electric power calculated by:

$$Qt = V \times I \quad (3)$$

The convection heat transfer from the surface:

$$Q_{conv.} = Q_t - Q_{cond} - Q_{rad} \quad (4)$$

Where, Q_{rad} is the losses in radiation heat transfer, which could be ignored as the temperature difference between the temperature of the plate and the temperature of the air were small [31]. Q_{cond} is the total losses in conduction heat from the bottom surface of the heater, the convection heat flux calculated by:

$$h_{Exp} = \frac{Q_{conv.}}{A_s(T_{pm}-T_{bm})} \quad (5)$$

Where As is the surface area for the plate. The local Nusselt number can be determined as:

$$Nu_{Exp} = \frac{h_{Exp}\, D_h}{k} \quad (6)$$

Where D_h is the hydraulic diameter and get by:

$$D_h = \frac{4A}{P} = \frac{4(H*W)}{2(H+W)} \quad (7)$$

Where A is the area of the inlet section and P wetted perimeter of the cross-section. Reynolds numbers depends on the hydraulic diameter (Re_{D_h}) as:

$$Re_{D_h} = \frac{u_\infty D_h}{\upsilon} \quad (8)$$

To find the numerical heat transfer coefficient hNum and numerical Nusselt number NuNum, It can be noted theoretically that Fourier's law and Newton's law at the surface (y=0) are combined [32], and the local coefficient of the heat transfer is:

$$h_L = -k\frac{\partial T(x,0,z)/\partial y}{(T_S-T_\infty)} \quad (9)$$

Where, Ts is surface temperature and T_∞ is the air temperature away from the plate surface. The average heat transfer coefficient can be obtained by integrate the local coefficient of heat transfer along the plate as:

$$\bar{h} = \int_0^x \int_0^z h_L \; dzdx \quad (10)$$

And numerical Nusselt number Nu_{Num} can calculated as:

$$Nu_{Num} = \frac{h_{Th}\, D_h}{k} \tag{11}$$

The friction factor was calculated from the air velocity (u) and the pressure loss (ΔP), which measured across the length of test section, using Darcy Weisbach equation as, [3]:

$$f = \frac{1}{2}\frac{\Delta P}{\rho u^2}\frac{D_h}{L} \tag{12}$$

$$\Delta P = P_{inlet} - P_{outlet} = 9.81 * \Delta h * \rho_m * \cos\theta \tag{13}$$

Where P_{inlet} and P_{outlet} are the pressures of the inlet and outlet and sections of the test section, Δh is the height of the inclined manometer, ρ_m is the density of the manometer liquid and θ is the angle of the inclined manometer.

2.2 Uncertainty analysis

The accuracy of the experimental result depends on the precision of individual devices and manufacturing accuracy of the device. Holman [33] described the approximation methods that used to calculate the uncertainty for the Reynolds number and heat transfer coefficient. The total uncertainty for the inlet velocity of the air, pressure drop along the channel, inlet temperature of the air, outlet temperature of the air, mean temperature of the plate surface, input power to the heater, rate of heat transfer, plate dimensions, dimension of the ribs, heat losses and were ±3.92%, ±6.4%, ±3.51%, ±4.59%, ±5.4%, ±3.82%, ±3.87%, ±0.91%, ±0.87% and ±1.77%, respectively. These combined to present a maximum error of 3.20% in Nusselt number with a maximum error of 3.05% in all Reynolds numbers.

2.3 Validation of the work

Validation should be made prior to confirm the results of the smooth tube; this verification will give a confidence for the final numerical results of the cases. The validation was present for the tests of fluid flow in the smooth channel only as depicted in Figure 4(a) with Yang et al [30] that produced a correlation equation (14) of Nusselt number for the smooth plate. This equation compared with the values of numerical and experimental for the smooth channel with an error about 7.45% and 9.09% respectively. While the friction factor equation (15) which presented by Yunus [34] for the rectangular channel at a width to height ratio is 2 and validated with the experimental and numerical results for smooth channel and the errors where 10.51% and 8.65% respectively as shown in Figure 4 (b). This deviation occurs from the assumptions, the approximations and the numerical error.

$$Nu_0 = 3.12 + 0.003\ Re_{Dh} \tag{14}$$

$$f_0 = 62.2 / Re_{Dh} \tag{15}$$

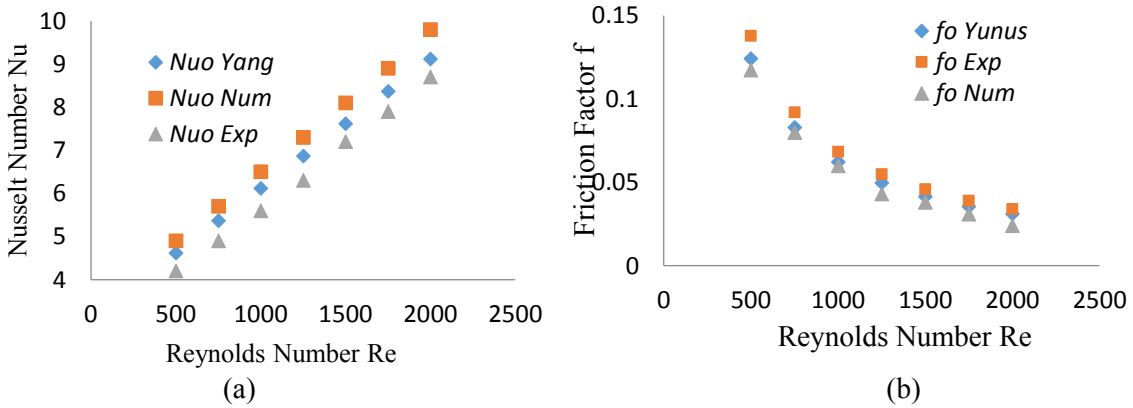

Figure 4. Validation of (a) Nusselt number and (b) Friction factor for smooth channel.

For the ribbed surfaces, an additional verification was produced to corroborate and ratify the results of the numerical outcomes with the experiment results of the work. Table 2 shows a comparison between the measured pressure drops of the experimental results for all models with those numerical results for roughness pitch (p/e) of 10, roughness height (e/D_h) of 0.06 and blockage ratio (e/H) of 0.08 and give good notarized results.

Table 2. Experimental and numerical pressure drop results.

Reynolds number	Δp Exp (Pa)				Δp Num (Pa)				Max. Error %
	500	1000	1500	2000	500	1000	1500	2000	
Smooth Plate	0.0506	0.1692	0.4265	0.7273	0.0542	0.1798	0.445	0.775	7.11
Model 1	0.052	0.1781	0.4561	0.8186	0.0565	0.1891	0.4911	0.871	8.65
Model 2	0.0556	0.187	0.4805	0.8254	0.061	0.1971	0.5151	0.860	7.91
Model 3	0.0566	0.1928	0.4961	0.8537	0.061	0.2071	0.5280	0.8911	7.77
Model 4	0.0503	0.1701	0.4315	0.7445	0.0542	0.1789	0.4611	0.7650	7.75
Model 5	0.0519	0.1752	0.4505	0.78	0.0565	0.1851	0.4850	0.7989	8.86
Model 6	0.0518	0.1771	0.4513	0.7712	0.055	0.1889	0.4749	0.8131	6.17
Model 7	0.051	0.1719	0.4413	0.7579	0.055	0.1850	0.4750	0.7990	7.84

3. Numerical analysis

3.1 Description of cases geometry

The channel length to hydraulic diameter ratio (L/D_h) is 3. Channel aspect ratio (W/H) is 2. The ribs were tested with rib height to duct hydraulic diameter ratio (e/D_h) is 0.06 and rib width to hydraulic diameter (Wr/D_h) is 0.15, the rib turbulators were rectangular cross section rods (e=H=10 mm and Wr=25 mm). The ribs fixed at different locations on into seven models listed in Table 1 and shown in Figure 5.

3.2 Mesh generation

ANSYS CFX 14.0 program were used to explore the heat transfer phenomena in several engineering fields and applied to realize the numerical analysis effect of ribs on the airflow profile and their arrangement on the thermal performance of the system [20].

ANSYS MESHING ICEM CFD 14.0 is the program acting to produce the meshing process. Automatic elements owning 4 nodes was applied. At each node of element possessing three degrees of freedom in three dimensional with keep the mesh parameters aspect ratio, mesh smooth and the angle of the skewness ratio that collected to be 1%, 20% and 0.78, respectively.

Grid Convergence Index (GCI) presented to validate the quality of the mesh [35]. The spaces of the mesh in three dimensions tested for every case as 0.5, 0.3 and 0.1 mm and the GCI's were 0.521 and 0.101mm respectively as is shown in Figure 6. The finer meshes give highly accurate and stability values, and thus 0.1 mm mesh spacing was chosen. For reliability in the discretization scheme, any density decreasing of the grids will increase the errors, so that the number of the elements number has a significant factor to reach the mesh independence result compared with the bulk fluid temperature. Therefore, the limits of the grid density in this work for all cases were between 1124521 and 1487214, as shown in Figure 7.

Commercial code of ANSYS CFX 14.0 [36] used to create the fluid flow model of smooth and ribbed channels. SIMPLEC (Semi-Implicit Method for Pressure-Linked Equations-Consistent) algorithm produced to solve the Navier Stokes equations using coupling the pressure and velocity. Second order upwind selected for calculating the momentum and energy whereas the standard format selected for pressure discrete arrangement. To achieve the convergence conditions the quality residuals are about 1×10^{-6} while the value of energy residual is about 1×10^{-9}. For all cases, the Reynolds number ranges were 500-2000. The simulations heater is selected of Aluminum wall with constant heat flux, time-independent, with constant physical properties of the air, which enters at temperature 300K, and out to the atmospheric pressure.

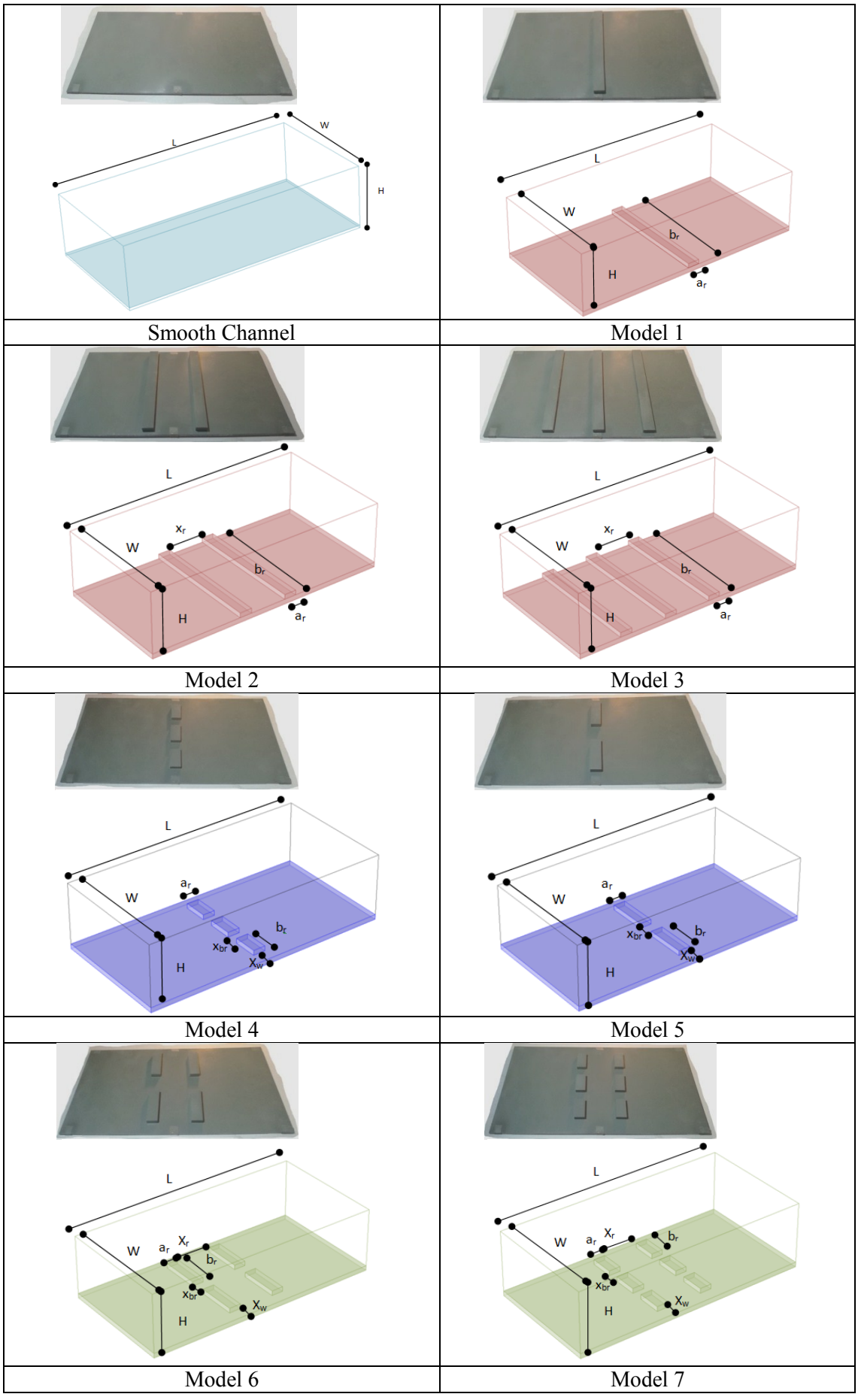

Figure 5. Experimental arrangement cases.

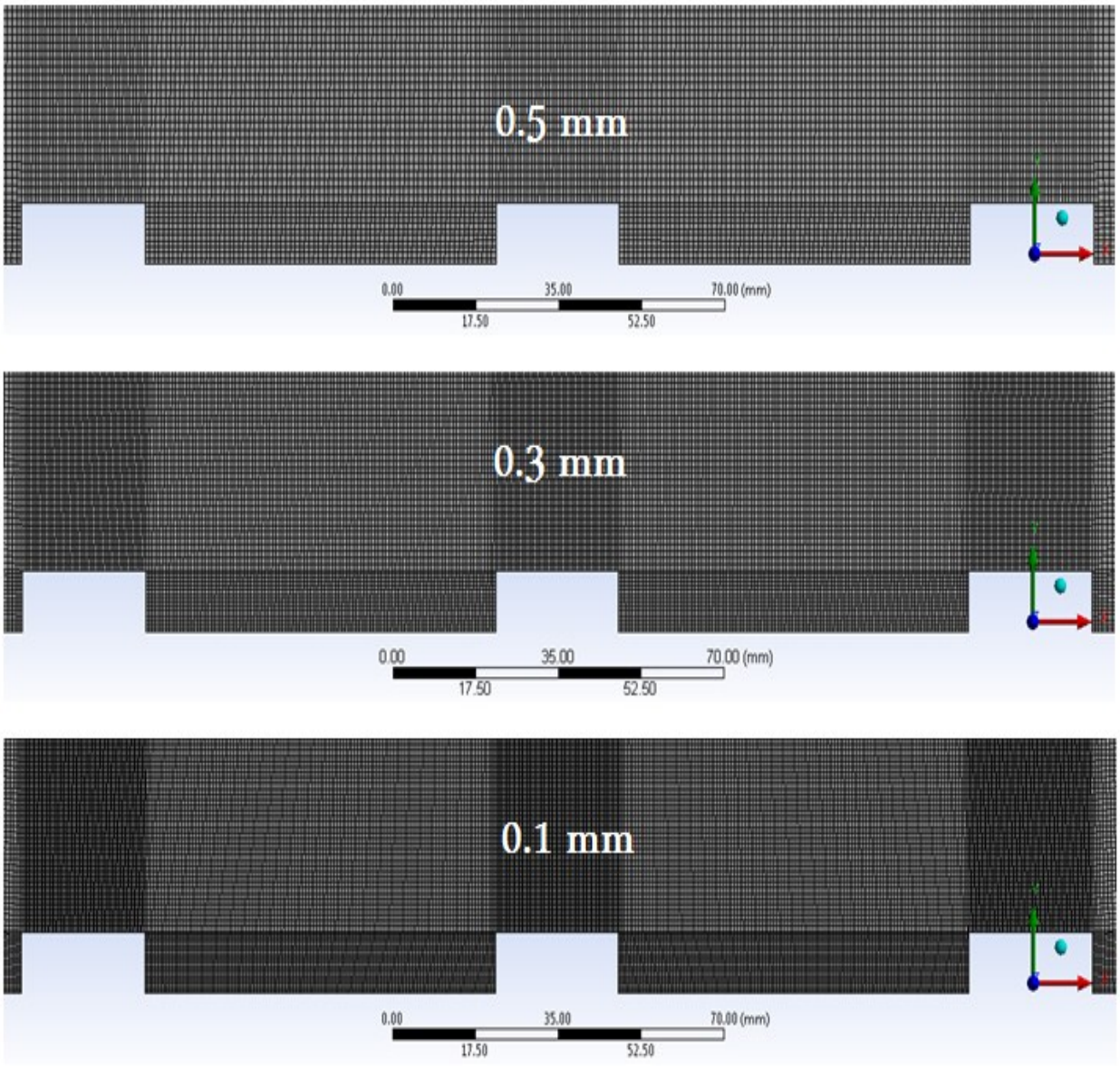

Figure 6. Process of grid refinery.

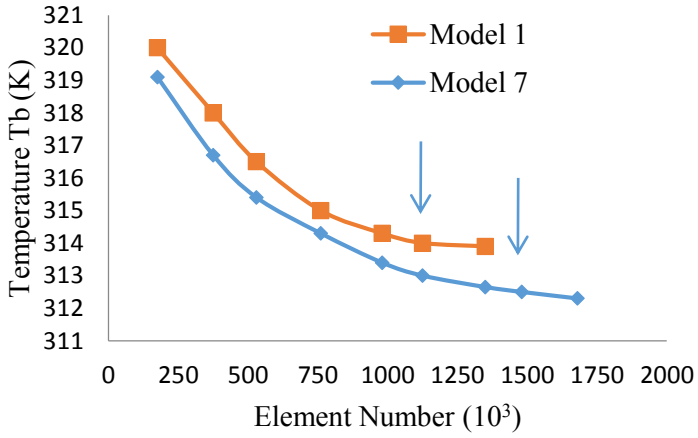

Figure 7. Element number vice bulk temperature.

3.3 Numerical modeling

Navier-Stokes equation plays an important role for simulation of CFD problems, the governing equations are [1]:

$$\frac{\partial U}{\partial X}+\frac{\partial V}{\partial Y}+\frac{\partial W}{\partial Z}=0 \tag{16}$$

$$\frac{\partial(UU)}{\partial X}+\frac{\partial(VU)}{\partial Y}+\frac{\partial(WU)}{\partial Z}=-\frac{\partial P}{\partial X}+\frac{1}{Re}\left(\frac{\partial^2 U}{\partial X^2}+\frac{\partial^2 U}{\partial Y^2}+\frac{\partial^2 U}{\partial Z^2}\right) \tag{17}$$

$$\frac{\partial(UV)}{\partial X}+\frac{\partial(VV)}{\partial Y}+\frac{\partial(WV)}{\partial Z}=-\frac{\partial P}{\partial Y}+\frac{1}{Re}\left(\frac{\partial^2 V}{\partial X^2}+\frac{\partial^2 V}{\partial Y^2}+\frac{\partial^2 V}{\partial Z^2}\right) \tag{18}$$

$$\frac{\partial(UW)}{\partial X}+\frac{\partial(VW)}{\partial Y}+\frac{\partial(WW)}{\partial Z}=-\frac{\partial P}{\partial Z}+\frac{1}{Re}\left(\frac{\partial^2 W}{\partial X^2}+\frac{\partial^2 W}{\partial Y^2}+\frac{\partial^2 W}{\partial Z^2}\right) \tag{19}$$

$$\frac{\partial(U\theta)}{\partial X}+\frac{\partial(V\theta)}{\partial Y}+\frac{\partial(W\theta)}{\partial Z}=\frac{1}{PrRe}\left(\frac{\partial^2 \theta}{\partial X^2}+\frac{\partial^2 \theta}{\partial Y^2}+\frac{\partial^2 \theta}{\partial Z^2}\right) \tag{20}$$

Where: $X = x/H,\ Y = y/H, W = w/H, U = u/u_\infty, V = v/u_\infty, W = w/u_\infty,\ \theta = (T - T_\infty)/(T_w - T_\infty)$ and $P = p/\rho u_\infty^2$ as u_∞ and T_∞ are the inlet velocity and inlet temperature of the air flow respectively. Prandtl number is the dimensionless parameter, which defined as:

$$Pr = \mu\ C_p/k \tag{21}$$

3.4 Boundary conditions and assumptions

The boundary conditions for all the boundaries of the flow domain with dimensionless are the components of the velocity (U,V,W), temperature (T), and pressure (P) can be described with the normal vector (n) as:
The inlet condition: U=1, V=W=0, ∂P/∂n=0 and $\theta = 0$
The outlet condition: ∂U/∂n= ∂V/∂n= ∂W/∂n=0, P=0 and $\partial\theta/\partial$n=0
The top and side walls: U=V=W=0, ∂P/∂n=0 and $\partial\theta/\partial$n=0
The bottom and ribs wall: U=V=W=0, ∂P/∂n=0 and $\partial\theta/\partial$n = -q"/k

There are some assumptions could be considered as:

a. The cooling fluid is dry air and flows in three-dimension as laminar flow, Newtonian fluid, time-independent and incompressible flow.
b. Dirichlet no-slip boundary conditions at the heater and rib walls subjected to momentum field.
c. Thermophysical properties of the air are constant.
d. Irreversible dissipation from kinetic to thermal energy were neglected.
e. The temperature of the top and sidewalls are constant.
f. Neglect radiation energy transfer and the viscous dissipation.

4. Results and analysis

4.1 Heat transfer results

The effect of Reynolds number along with the smooth channel and the other models on the values of the Nusselt number expressed in Figure 8. It can be shown in all cases, the increasing of Nusselt number with the Reynolds number. This explained as the inlet velocity of the air increases, the mass flow rate enters the test section will increase, and Reynolds number increases too. This will causes a reduction in the temperature of the plate because the heat at the surface will transfer at a higher rate and the heat transfer coefficients will increase, therefore the local Nusselt number augments with the Reynolds number directly. On the other hand, the temperature values of the hot plate increases with the rise in the heater power. Again for all cases it can be noticed that the local Nusselt number declines along the plate length, this is because of the boundary layer will grow along the plate and the local velocity near the plate reduces, therefore the temperature will raises downwards the plate and the heat transfer coefficient will decrease therefore the local Nusselt number decreases. In all cases, the ribbed surfaces have a significant effect and the heat transfer is higher than the smooth surface.

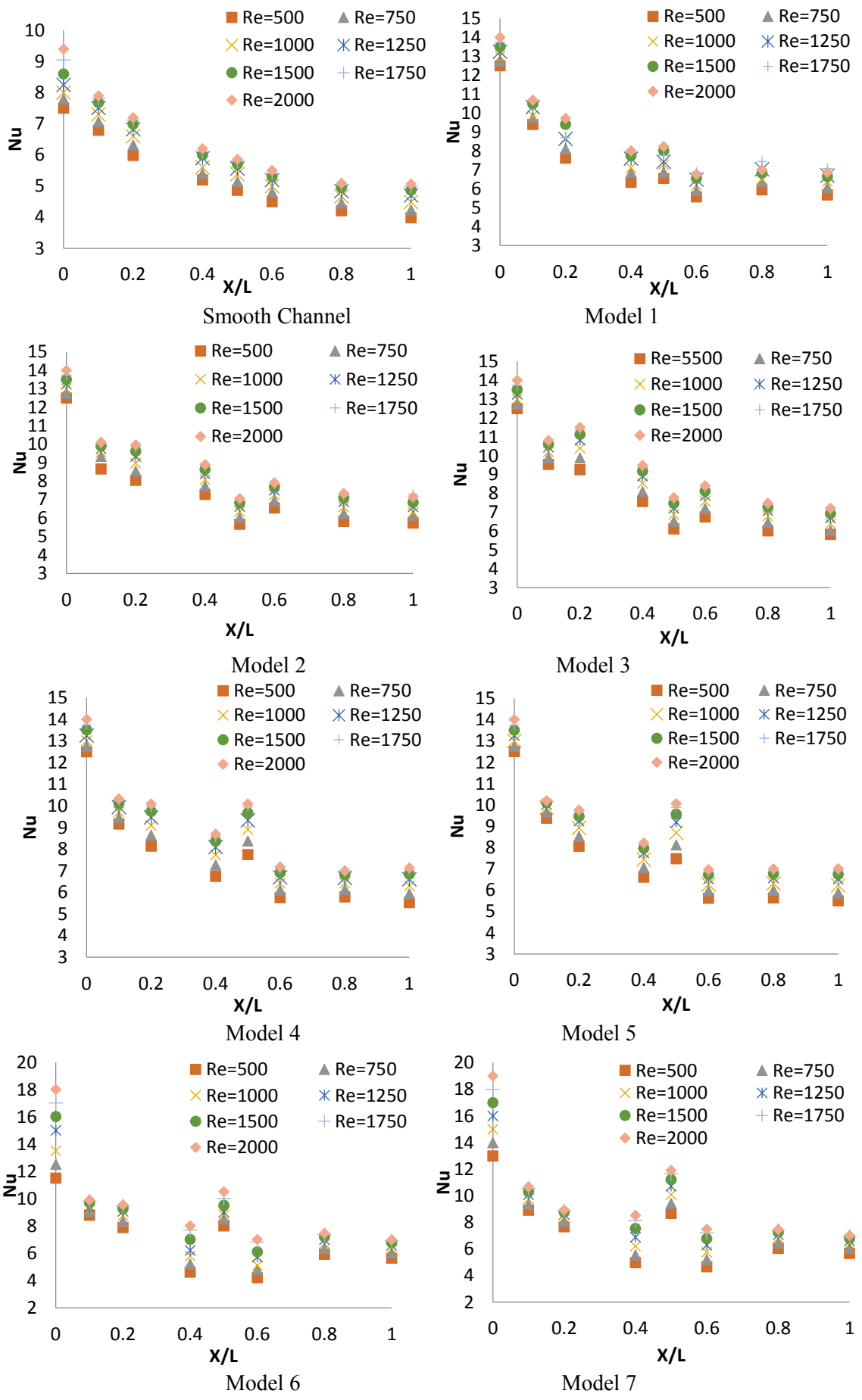

Figure 8. Nusselt number distribution along the channel of the all models.

For the models 1, 2 and 3, it can be noticed in Figure 9, that the Nusselt number effects with the number of rows along the plate. The Figure shows the values of Reynolds number 500, 1000, 1500 and 2000. It can be shown as the Reynolds number increases, the local Nusselt number for all cases increases too. The ribs break the laminar boundary layer along the plate and form local turbulence between the ribs; without significantly disturbing the main airflow; and the flow reattachment the shear layer this will produce the air to move away the heat from the hot plate. The rib creates separation section on each sides of the rib and hence the heat transfer enhanced as well as the friction factor happens. Therefore, it can be noted that the three ribs are more effective than two and one ribs.

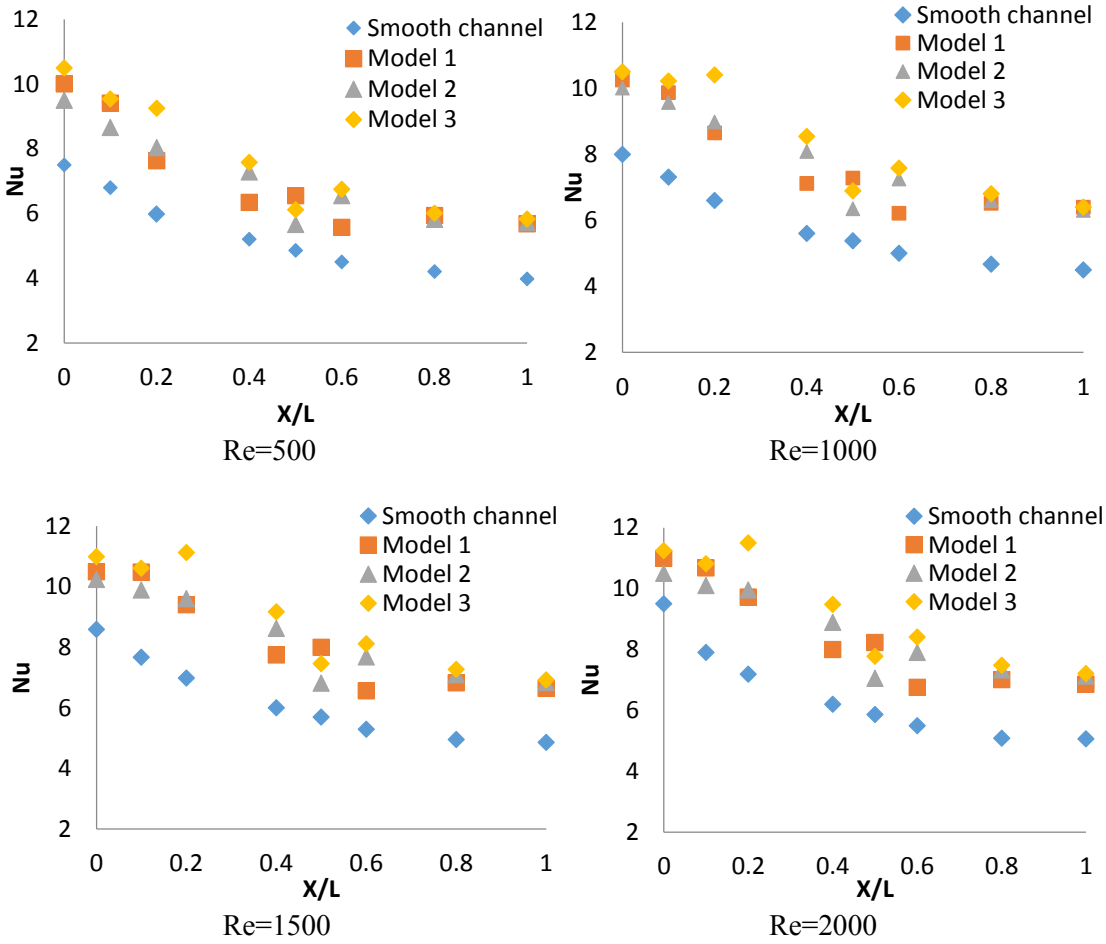

Figure 9. Effect of number of ribs on Nu distribution along channel length.

The effects of the discretization of the single rib into two and three separated parts are shown in Figure 10 to compare the model 1, 4 and 5. The Figure gives details of the values of Reynolds number be 500, 1000, 1500 and 2000. Again, the local Nusselt number generally increases with the Reynolds number as mentioned above. The airflow through the split rib and the boundary layer breaks down between the spaces this will create more turbulence; the heat transfer coefficient will be higher for the model 4 than the model 5 and 1, and conclude that the three parts are more efficient. So that the model 2 was developed to estimate the behavior of the airflow through parallel ribs parted into two and three parts in inline arrangement as it clearly shown in Figure 11 for different values of Reynolds number (500, 1000, 1500 and 2000). The model 6 and 7 declared that the three parts are more efficient than single and two parts and the local Nusselt number increases as the airflow enters through the gaps which cause more turbulence among consecutive ribs in addition to the separation and reattachment of the shear layer between two rows of detached ribs.

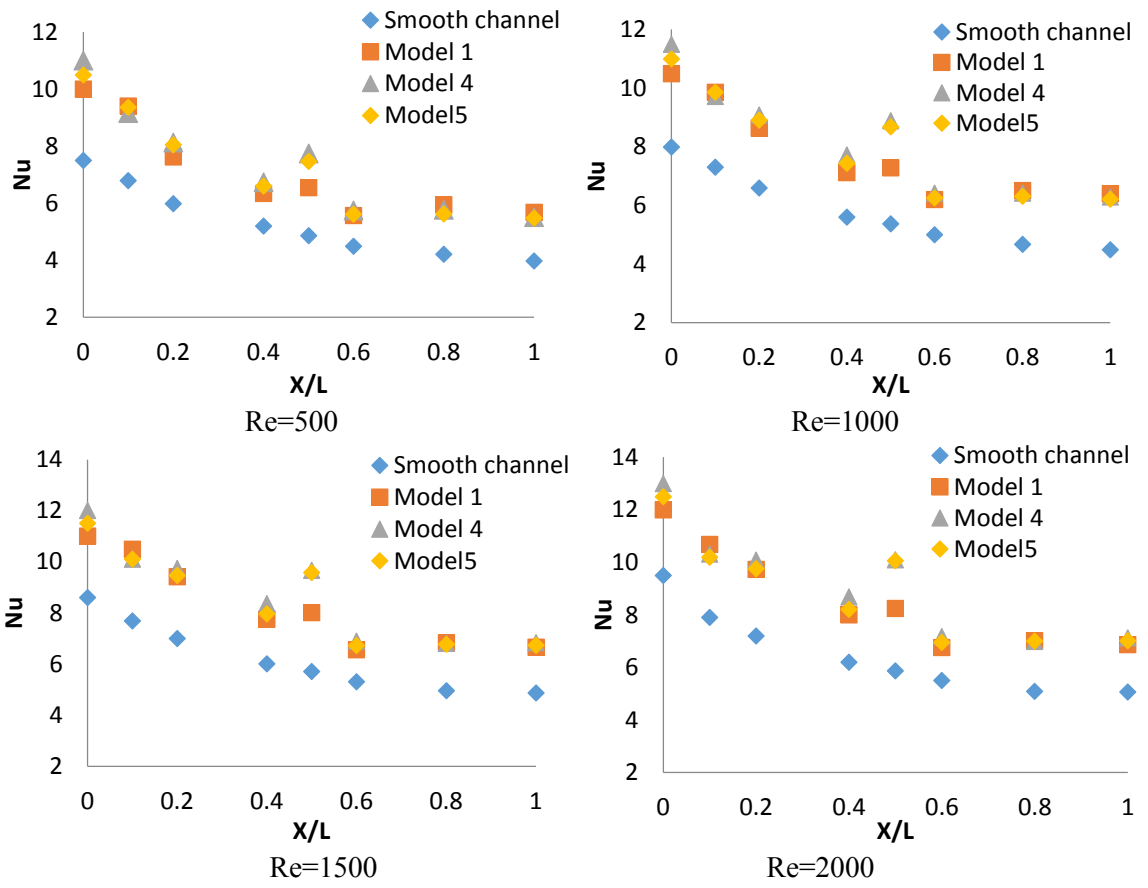

Figure 10. Effect of parting of one solid rib on Nu distribution along channel length.

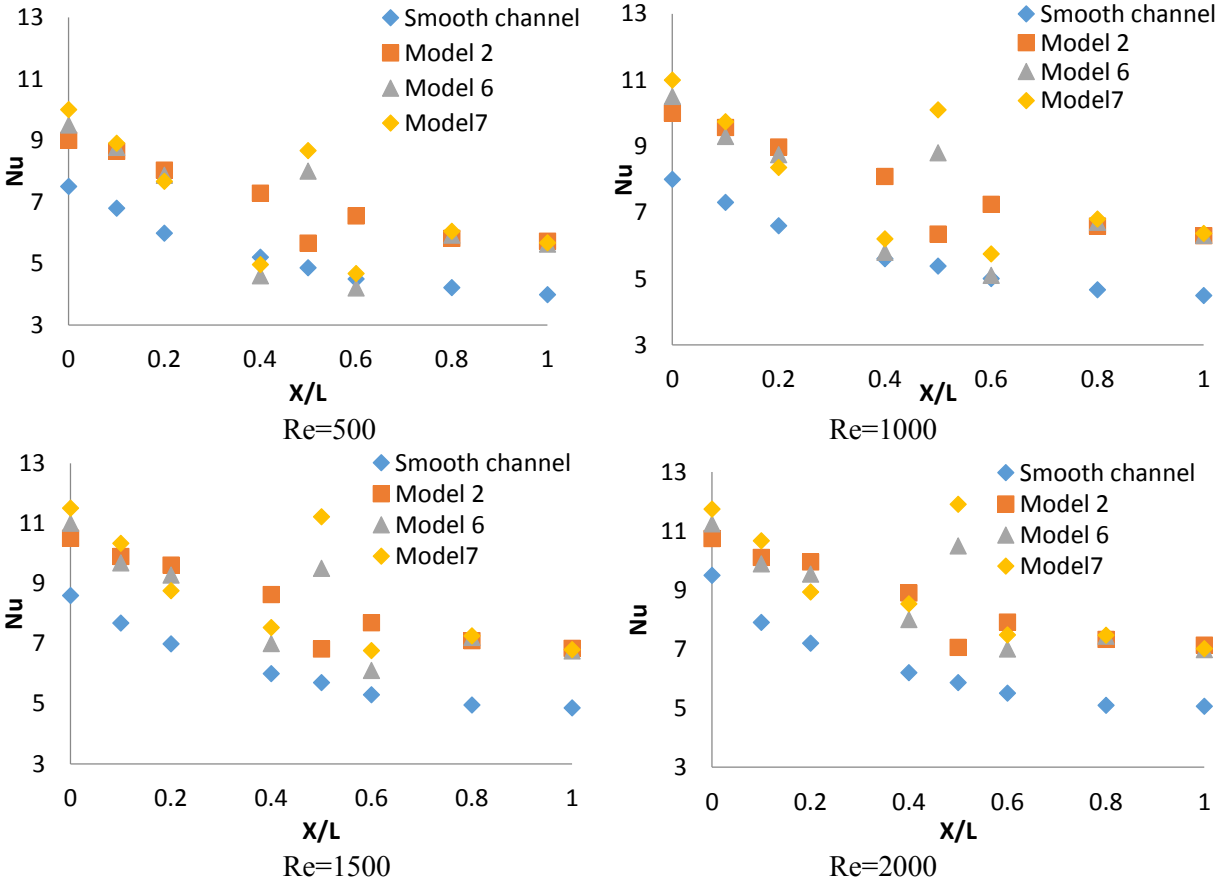

Figure 11. Effect of two solid ribs on Nu distribution along channel length.

4.2 Pressure drop results

Figure 12 shows the pressure drop along the test section for the ribbed surface compared with the smooth surface. Generally, It can be shown that the adding of ribs will increase the pressure drop for all seven models as the flow will stop completely in front of the rib so that pumping power increases and consequently the friction factor (pressure drop) for the model 3 is higher than model 2, and 1 as it clear in Figure 12(a). While Figure 12(b) shows the pressure drop along the test surface with the effect of dividing the rib into one, two and three parts. The airflow between the parts of the ribs and the air in front of ribs turn and take side passage parallel to the side wall of the rib, this will decrease the pressure drop along the test section and hence the friction factor too. Therefore, the three parts have lower value than the two parts and the continuous rib will produce a higher value. Figure 12 (c) shows the effect of the parting of ribs in the two parallel ribs on the pressure drop. The model 7 has lower value in pressure drop compared with model 6 and 2 as the air passage between many numbers of gaps of the inline rows in model 7 than the others.

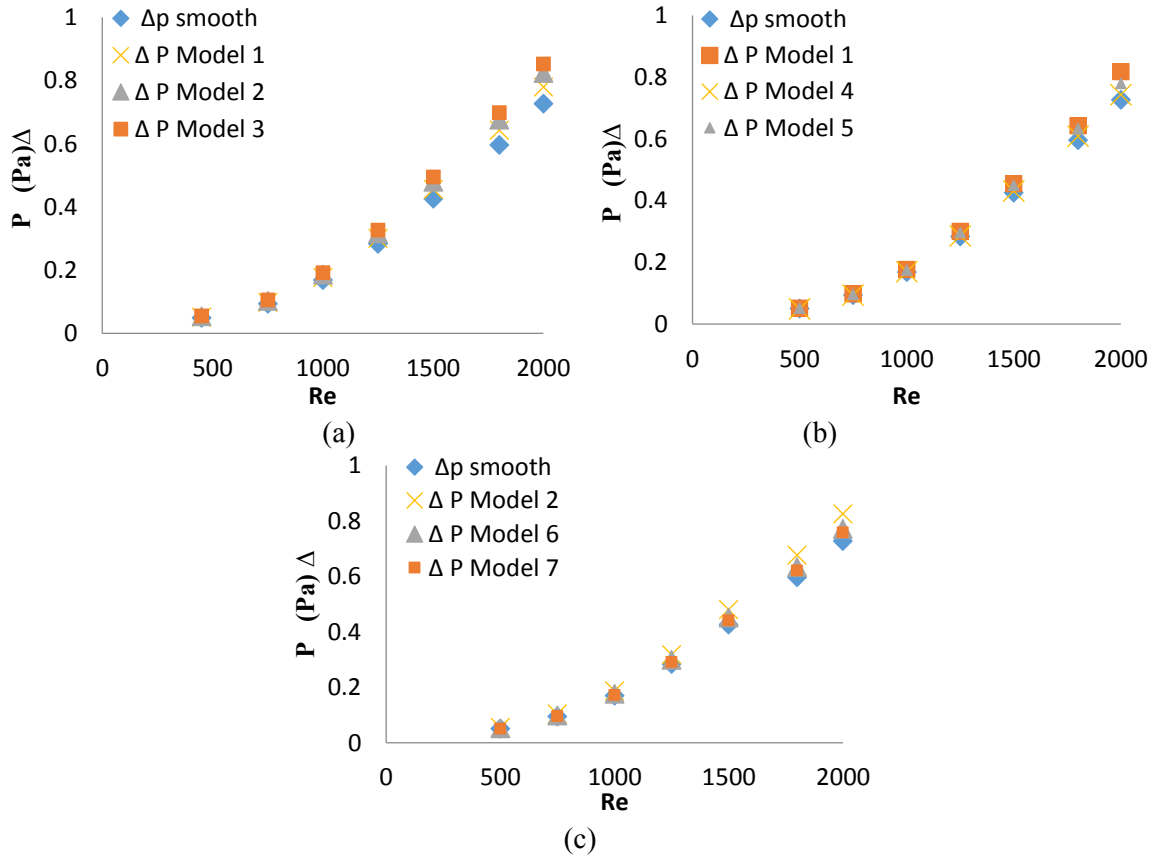

Figure 12. Effect of (a) Number of ribs, (b) Parting of one rib and (c) Parting of ribs in the two parallel ribs on the pressure drop.

4.3 Overall enhancement ratio

The important objective function is to enhance the Nusselt number and to decrease the pressure loss. Overall enhancement ratio demonstrates the heat transfer accomplished by the pumping power (or pressure drop). Thermal performance factor or overall enhancement ratio defined by Webb and Kim [1] overall enhancement ratio as:

$$\text{Overall Enhancement Ratio } \eta = \frac{\text{Nu}}{\text{Nu}_o} \Big/ \left(\frac{f}{f_o}\right)^{\frac{1}{3}} \quad (22)$$

Where, Nuo and fo are average Nusselt number as well as the friction factor for the smooth channel.

4.3.1 Effect of the ribs number

Figure 13 shows the effect of Reynolds number on Nusselt number ratio (Nu/Nuo) and friction factor ratio (f/fo) and the overall enhancement ratio for model 1, 2 and 3 to explain the effect of the number of ribs on

the heat transfer phenomena. The Figure shows that the Nusselt number ratio for model 3 is 2.15 than the smooth channel, which is higher than the others, that is mean as the number of ribs along the test section increase, the Nusselt number ratio increases. on the other side, the friction factor ratio of the model 3 has 2.18 than the smooth channel which is the highest value than the other models. The Figure shows the overall enhancement ratio for model 1,2 and 3. It can be shown there is a significant effect of the ribs on the overall enhancement ratio for all values of Reynolds number. The overall enhancement ratio increase directly with Reynolds number until Re=1500 to reach 1.68, after that the overall enhancemnet ratio decreases slightly to get 1.67 at Re=2000, as the friction factor have a significant effect and the pumping power increases. These is compared with the results produced by Alam and Kim [20] and Gawande et al [22] and get the same conclusions. The best type is model three and the overall enhancement ratio was 1.68 at Reynolds number is 1500.

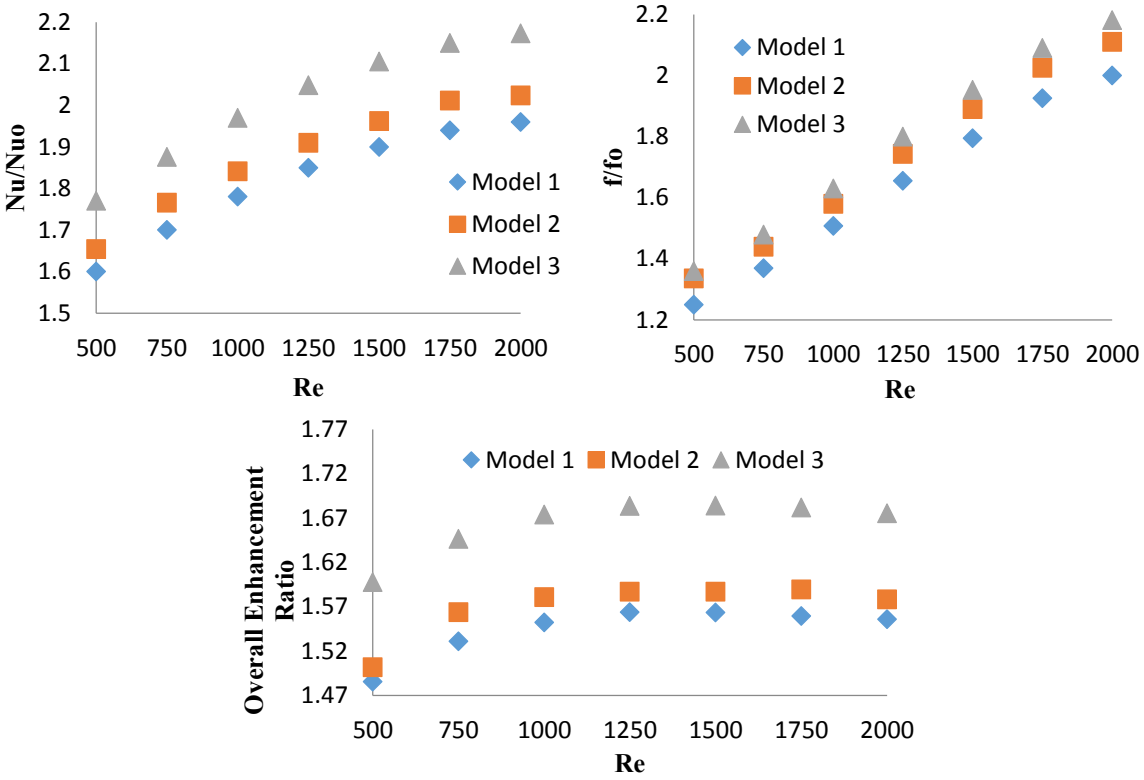

Figure 13. Effect of the number of rib on f/f_o, Nu/Nu_o, η ratios for models 1, 2 and 3.

4.3.2 Effect of discrete of single rib

Figure 14 shows the effect of Reynolds number on Nusselt number ratio (Nu/Nuo) and friction factor ratio (f/fo) and the overall enhancement ratio for model 1, 4 and 5 to explain the effect of the discrete of the rib into parts. It can be shown clearly that the Nusselt number ratio for the three parts has a higher value 2.096 than the others with the minimum value of friction factor ratio. So that the overall enhancement ratio higher compared with the other models and be 1.709 at Reynolds number about 1500 and declare slightly to be 1.69 at Re=2000.

4.3.3 Effect of parting for inline ribs

Figure 15 shows the effect of Reynolds number on Nusselt number ratio (Nu/Nuo) and friction factor ratio (f/fo) and the overall enhancement ratio for model 2, 6 and 7 to explain the effects of the inline ribs discrete into two and three parts. It can be obvious that the Nusselt number ratio for the model 7 has the best value and reach 2.17 at Reynolds number 1500 with least value of friction factor ratio. Thus the overall enhancement ratio higher measured up to the other models and be 1.736 at Reynolds number about 1500 and declare a little to 1.626 at Re=2000. The shape of the curves result of the discrete of the single rib and parted ribs of inline rows compared with the laminar range of Yang et al [30] and gives good agreement.

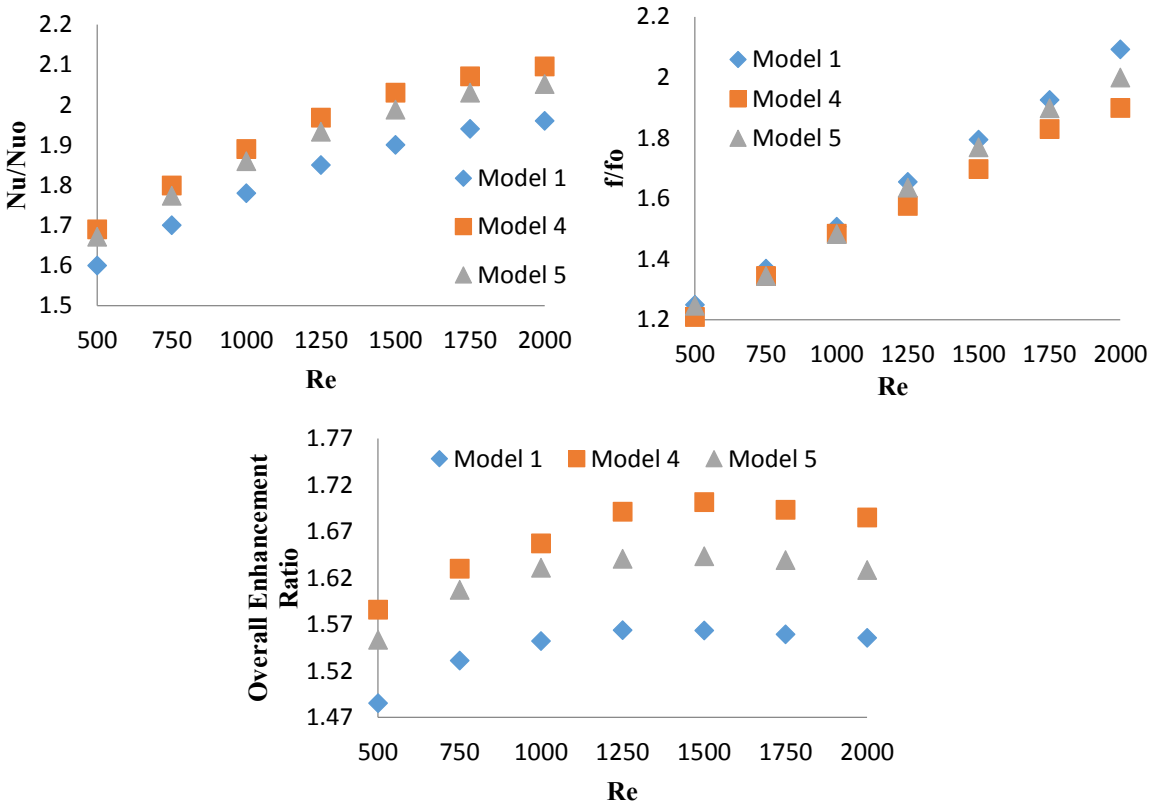

Figure 14. Effect of parting of one rib on f/f_o, Nu/Nu_o, η ratios for models 1, 4 and 5.

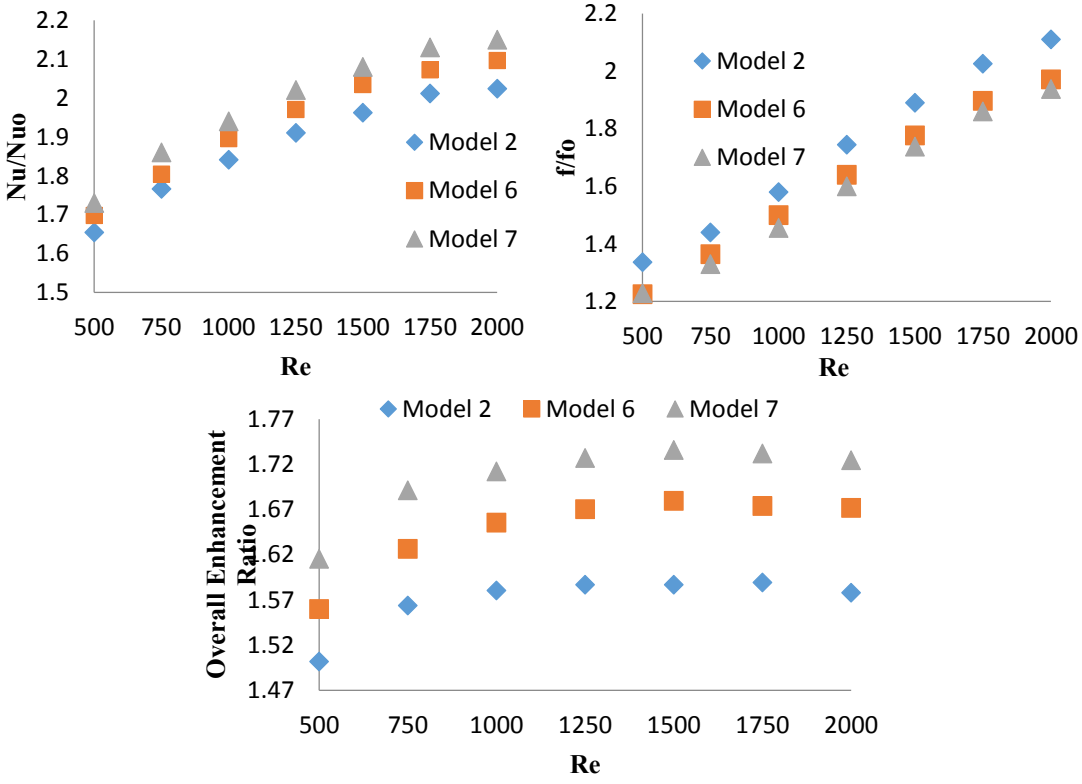

Figure 15. Effect of parting of two parallel ribs on f/f_o, Nu/Nu_o, η ratios for models 2, 6 and 7.

Figure 16 illustrates the profile of the streamline through the channel achieved from numerical simulation at Reynolds number 500,1000,1500 and 2000 and roughness pitch p/e=10. There are many regions between ribs, which are the separation state, reattachment state and the flow over flat state after the rib. It can be

noticed that the mass flow rate effect on the profile of the streamline and there is a separation region generates in the groove between the ribs that forms a separation vortex, the flow reattaches to the rib wall inside the groove.

Acoording to the verfications in Table 2 which gave a good agreement between the experimenat and numerical results, numerical work was extented the to cover a wide range more than those of the experimental work as relative roughness picth p/e=10 and the blockage ratio e/H=0.08. The numerical results for rib height selected as 8,10 and 12 mm and rib picth of 80,100 and 120 mm so the relative roughness ratio was 6.66<p/e<15.0, the blockage ratio range was 0.064<e/H< 0.096 and the relative roughness height be 0.048<e/D_h<0.072 and the Reynolds number range was 500<Re<2000; the new cases are mention in Table 3.

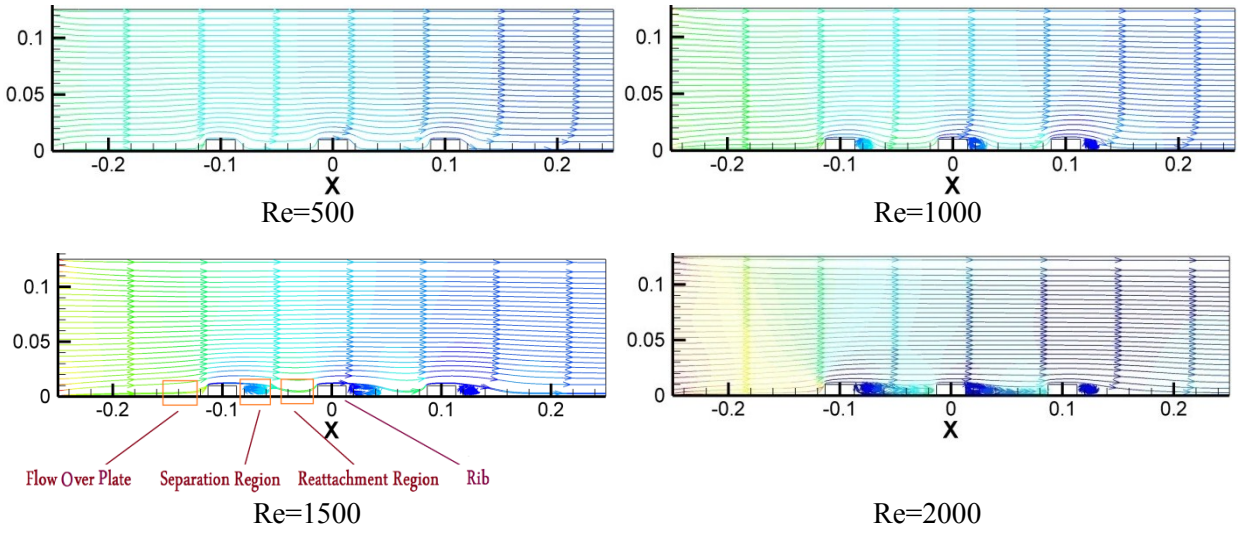

Figure 16. Streamline profile with Reynolds number at p=100mm and e=10mm (p/e=10).

Table 3. Parameters of the numerical calculation.

e	p	p/e	e/H	e/D_h
8	80	10	0.064	0.048
8	100	12.5	0.064	0.048
8	120	15	0.064	0.048
10	80	8	0.08	0.06
10	100	10	0.08	0.06
10	120	12	0.08	0.06
12	80	6.667	0.096	0.072
12	100	8.33	0.096	0.072
12	120	10	0.096	0.072

4.3.4 Effect of rib pitch to height ratio (relative roughness pitch)

Figure 17 shows the streamline profiles for the same height of the rib (e=10mm) and change the ribs pitch from 80, 100 and 120 so the roughness pitch were p/e as 8,10 and 12 with Reynolds number as 1000 and 2000. Figure 18 shows the Nusselt number with Reynolds number for the similar cases. The heat transfer coefficient at p/e=8 was between p/e=10 and 12, which indicates that the rib spacing effect on the heat transfer coefficient was not in a monotony augmenting with the rib spacing. When the air flows in ribbed channel, the major reasons to augment the convective heat transfer is the flow separation vortex after the rib and the reattachment to the wall. On the other hand, as the rib spacing increases, the effects of vortex separation and reattachment on the heat transfer is weak, but the effect of airflow above a flat area on convective heat transfer is step by step increased. When rib spacing is big p/e=12, the convective heat transfer of airflow above the flat is the major reason that controlling on the convective heat, which result in a decreasing the convective heat coefficient. However, the airflow reattachment will be slowly weakened since the reduce of rib pitch. When the rib pitch is small p/e=8, the airflow reattachment disappeared, cause a reduction in the coefficient of the heat transfer. Therefore, only when appropriating the rib spacing at

p/e=10, together of airflow separation vortex and the reattachment to the channel bottom could play a significant effects on the convective heat transfer coefficient, reaching to an optimal convective heat through the ribbed channel. The effect of the rib height e=8,10 and 12 mm at the same distance p=100mm on the Nu were shown in the Figure 19. It can be shown that the highest value of the heat transfer occurs at p/e=10 and the maximum heat transfer occurs for the reasons which explained before.

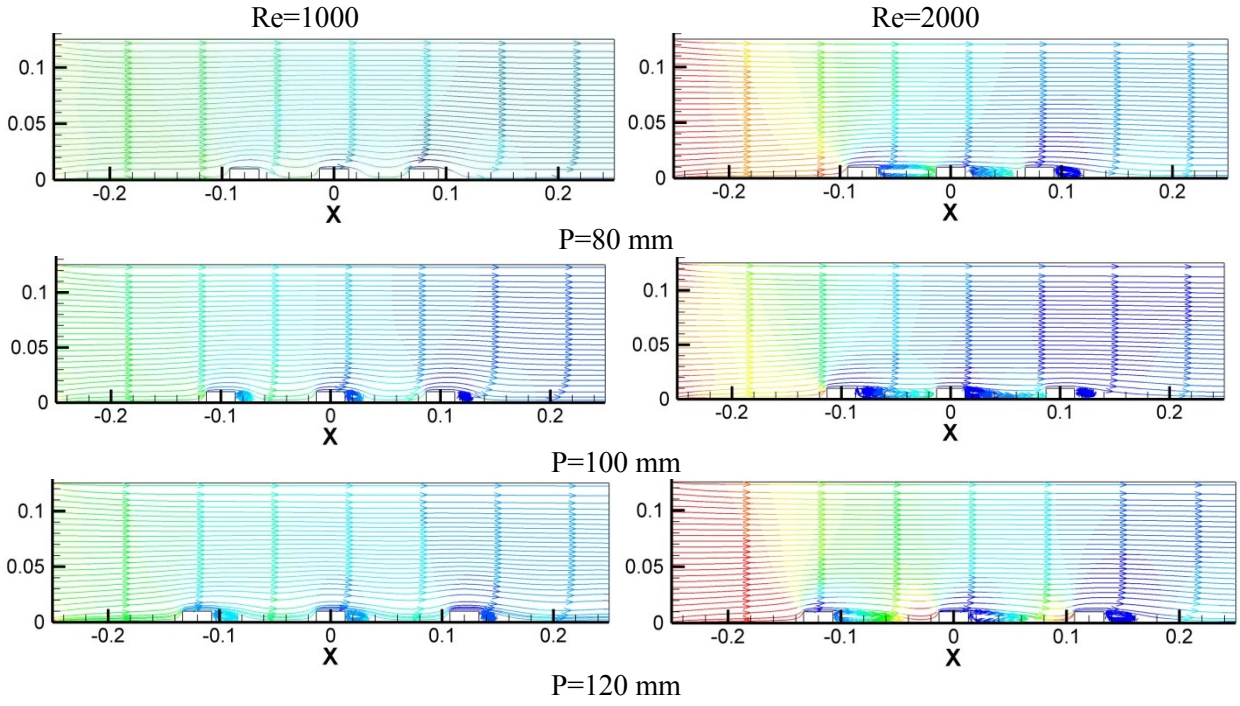

Figure 17. Flow fields at e=10mm, P=80,100 and 120mm apart and p/e=8,10 and 12 .

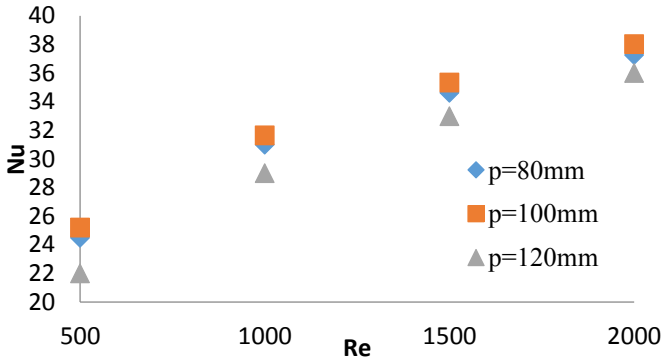

Figure 18. Nusselt number with Reynolds number for e=10mm and p=80,100 and 120mm.

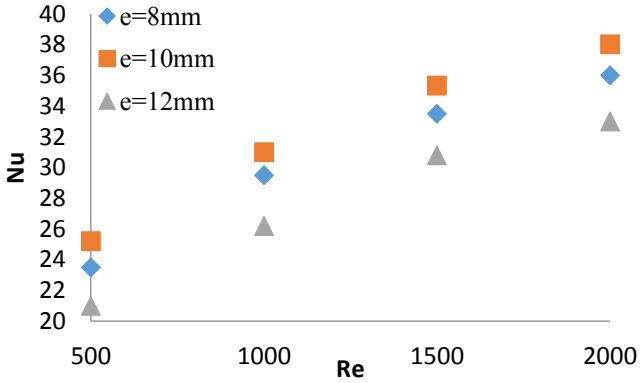

Figure 19. Nusselt number with Reynolds number for p=100mm and e=8,10 and 12mm.

4.3.5 Effect of rib height to channel height (blockage ratio)

The effect of the blockage ratio (e/H) on the streamlines of flow fields at P=80,100 and 120mm apart in ribbed channel with fixed ratio p/e=10 for Reynolds number of 1000 was produced in the Figure 20, the figure shows the streamline profile of the air flow over different values of ribs e=8mm (e/H=0.064) and e=12mm (e/H=0.096) and compare it with the streamline profile with the previous figure 16 of e=10mm (e/H=0.08) to cover the the whole range of p/e. It can be shown that, when the blockage ratio e/H is 0.096, the profile reveal a strong disturbance made by the rib, which forms a waved stream pattern which consequence in fluid separation within downstream of the rib with flow reattachment to the wall floor. Figure 21 shows the rib blockage ratio effects on the heat transfer which declared there is a significant effect on the Nusselt number and the Nusselt number increase with the blockage fraction. Therefore the Nusselt number of blockage ratio e/H= 0.096 is higher than the other values because of the air disturbance within the rib channel is considerably higher than the disturbance of the other blockage ratios which causes a higher heat transfer coefficient.

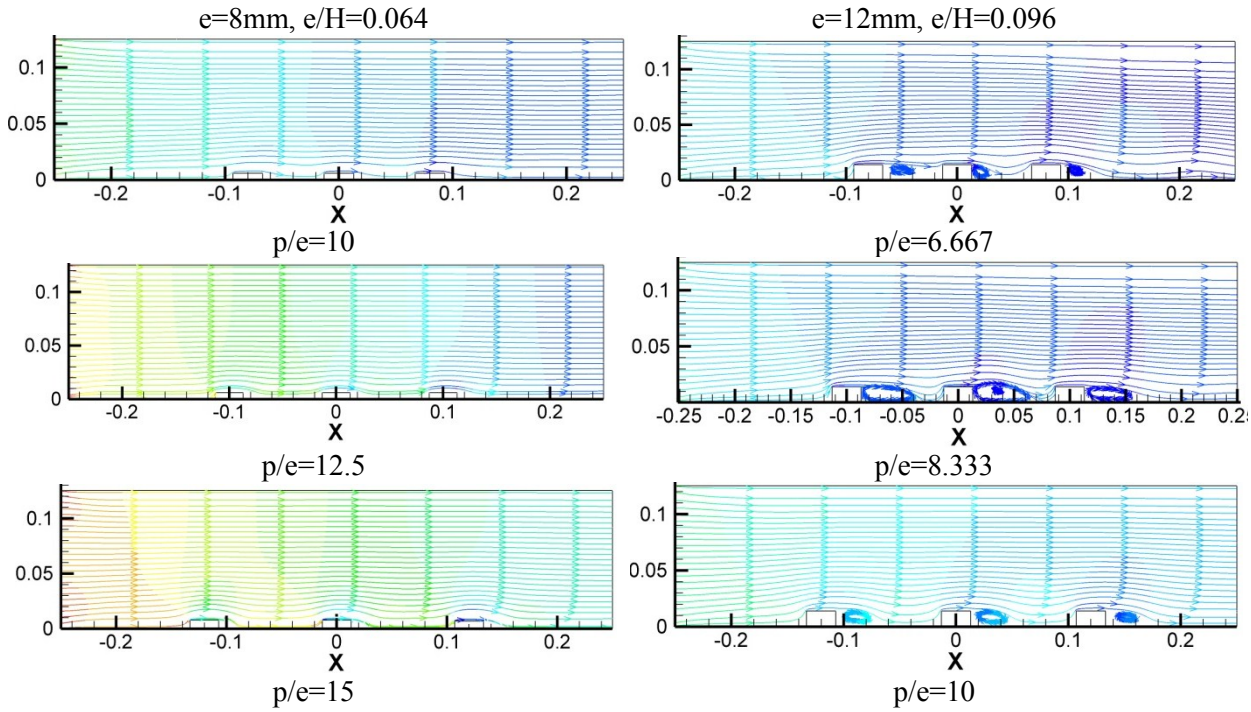

Figure 20. Flow fields at e/H=0.064 and 0.096 of Re=1000 and p=80,100 and 120mm apart and p/e=10.

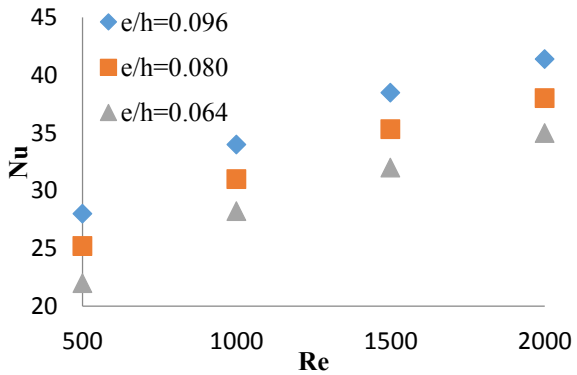

Figure 21. Nusselt number with Reynolds number for fixed p/e=10 and e/H=0.064,0.08 and 0.096.

As shown before, the heat transfer phenomena effects by many parameters as the geometry factors (rib height e, channel height H, and the rib pitch p) that means the relative ribs height, relative roughness pitch in additional to Reynolds number. Therefore the non-dimensional factors like e/H, p/e, Re are confirmed by Alam and Kim [20] as parameters of the criteria correlation equation. The common type can articulated as:

$$Nu=f\ (p/e,\ Re,\ e/H) \tag{23}$$

Alam and Kim [20] mentions the correlation equation may be displayed in power function as:

$$Nu= (p/e)^{a}\ (e/H)^{b}\ Re^{c} \tag{24}$$

The statistic program Microsoft Excel was used to deduce the output results for the cases of multi ribs (continuous and broken ribs) and get the correlation equation using Multiple Regression Analysis. The criteria of the study results are; the Multiple R=0.9997, Adjusted R Square=0.9688, R Square=0.9992and the Standard Error=0.0967. The criterion correlation equation of the Nusselt number is:

$$Nu= (p/e)^{0.111282}\ (e/H)^{-0.167207}\ Re^{0.40599} \tag{25}$$

This correlation equation is satisfied for airflow inside rectangular channel with $0.048\leq e/D_h\leq 0.072$, $6.66\leq p/e\leq 15$, $0.064\leq e/H\leq 0.096$ and $500\leq Re\leq 2000$. A comparison of Nusselt number between calculation and simulation results are shows in Figure 22. The deviation between these results is inside ±8%, and the correlation of the heat transfer calculations for rectangular ribbed channel is reliable.

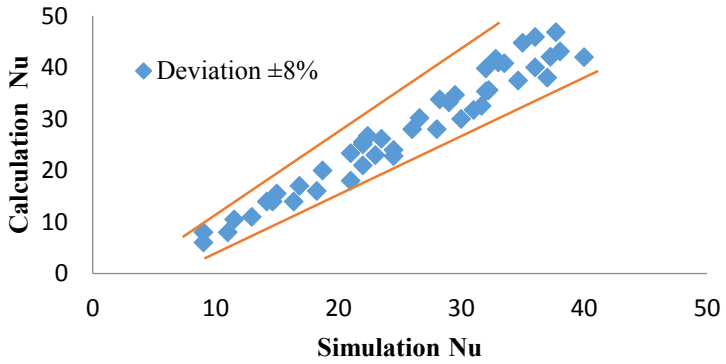

Figure 22. Comparison Nusselt number results.

5. Conclusions

The heat transfer phenomena and friction factor characteristic of the roughened plate has been investigated for seven models. The main conclusions are:

1- The ribs surface enhances the heat transfer for all models and the Nusselt number increases directly with Reynolds number. Nusselt number decrease gradually along the test section as the boundary layer grows and the friction factor increase.
2- The results show that the overall enhancement ratio was increased directly with Reynolds number until reaching the maximum value at Reynolds 1500 and decrease slightly until Reynolds number 2000 as the friction factor increases and the flow field reaches the transition flow regime. These results compared with the previous works and get good agreements.
3- For the models 1,2 and 3 it could be conclude that the number of the continuous rib increases the Nusselt number 1.93-2.15 times the smooth channel and friction factor increases as 1.98-2.18, but the overall enhancement ratio was 1.56-1.68 and the best type was model 3.
4- For the models 1,4 and 5, the partition of single rib into two and three parts, the effect of the Nusselt number ratio were 1.93-2.08 and the corresponding friction factor ratio were 1.98-2.09 to get the overall enhancement ratio was 1.56-1.69 so the finest type was the model 4.
5- For the models 2, 6 and 7 the array of two rows and discrete the ribs were had a significant action on the coefficient of heat transfer. The Nusselt number ratio was 2.02-2.17 while the friction factor ratio was 1.93-2.11 and the overall enhancement ratio was 1.58-1.736 and the best type was model 7.
6- The rib spacing had a significant effect on the heat transfer coefficient and the shear layer reattachment does not happen for a roughness pitch ratio of 8 as the flow separation downstream. The optimum heat transfer occurs at p/e of 10.
7- The blockage ratio had an efficient act on the heat transfer as the flow turbulance near the edge and and it works as turbulator, however, Nusselt number for e/H=0.096 is larger than the other values.
8- Heat transfer could be enhanced by rising the roughness height e/H for fixed relative roughness pitch p/e or by reducing the roughness pitch p/e at fixed roughness height e/H. Roughness pitch p/e could be augmented up to 10, further than there is a reduce in the heat transfer enhancement.

Nomenclature

A	Heated Surface Area (m^2)
Dh	Channel Hydraulic Diameter (m)
e	Rib Height (m)
h	Convective Heat Transfer Coefficient (W/K m^2)
f	Fanning Friction Factor
T	Temperature (K)
K	Thermal Conductivity (W/m K)
Re	Reynolds Number
Nu	local Nusselt Number
Pr	Prandtl Number
P	Local Pressure (N/m^2)
p_∞	Pressure as Coordinate Infinity (N/m^2)
P	Wetted Perimeter (m)
p	Rib Pitch (m)
Q	Heat Transfer Rate (W)
u_∞	Free Velocity Of Fluid (m/s)
u, v, w	Velocity Component in x,y,z Direction Respectively (m/s)
x , y, z	Cartesian Co. in Horizontal, Vertical, Depth Direction (m)
L	Length of the Rectangular Duct (m)
W	Wide of the Rectangular Duct (m)
H	Height of the Rectangular Duct (m)
Cp	Specific Heat Capacity (J/kg.K)

Subscripts

bm	Bulk Mean Fluid Temperature
pm	Mean Plate Temperature
t	Total
Conv	Convective Heat Flux (W/m^2)
Cond	Conduction Heat Flux (W/m^2)
Rad	Radiation Heat Flux (W/m^2)
In	Inlet
Out	Outlet
Exp	Experimental
Th	Theoretical
s	Surface
o	Smooth Plate
L	Local
n	Normal Vector
r	Rib

Greek Symbols

ρ	Density Of Fluid
ν	Kinematic Viscosity Of Fluid
μ	Dynamic Viscosity
θ	Angular Direction

References

[1] Webb, Ralph L. and Nae-Hyun Kim, "Principles of Enhanced Heat Transfer", 2nd Edition, Taylor & Francis Routledge, 2006.

[2] Karwa R, Solanki SC, Saini JS. Thermo-Hydraulic Performance of Solar Air Heaters Having Integral Chamfered Rib Roughness on Absorber Plates. Energy 2001, 26(2):161–76.

[3] Smulsky Ya.I., Terekhov V.I., Yarygina N.I., Heat Transfer in Turbulent Separated Flow Behind a Rib on The Surface of Square Channel at Different Orientation Angles Relative To Flow Direction, International Journal of Heat and Mass Transfer 2012, 55, 726–733.

[4] Du J., Yuxiang Hong, Si-Min Huang, Wei-Biao Ye, Shuangfeng Wang. 'Laminar thermal and flussid flow characteristics in tubes with sinusoidal ribs', International Journal of Heat and Mass Transfer 2018, 120, 635–651.

[5] Mahmood G.I., P.M. Ligrani, Heat transfer in a dimpled channel: combined influences of aspect ratio, temperature ratio, Reynolds number, and flow structure, Int. J. Heat Mass Transfer 2002, 45, 2011–2020.

[6] Saini RP, Verma J., Heat Transfer and Friction Factor Correlations for a Duct Having Dimple-Shape Artificial Roughness for Solar Air Heaters. Energy 2008, 33(8), 1277–87.

[7] Kovalenko G. V., V. I. Terekhov, A. A. Khalatov, Flow Regimes In A Single Dimple on The Channel Surface, Journal of Applied Mechanics and Technical Physics 2010, 51(6), 839–848.

[8] Wang L., B. Sunde´n, Performance comparison of some tube inserts, Int. Comm. Heat Mass Transfer 2002, 29, 45–56.

[9] Martemianov S., V.L. Okulov, on heat transfer enhancement in swirl pipe flows, Int. J. Heat Mass Transfer 2004, 47, 2379–2393.

[10] Suri A. R. S., Anil Kumar and Rajesh Maithani. Heat transfer enhancement of heat exchanger tube with multiple square perforated twisted tape inserts: Experimental investigation and correlation development. Chemical Engineering and Processing 2017, 116, 76-96.

[11] Won S.Y., G.I. Mahmood, P.M. Ligrani, Spatially-resolved heat transfer and flow structure in a rectangular channel with pin fins, Int. J. Heat Mass Transfer 2004, 47, 1731–1743.

[12] Dutta P., A. Hossain, Internal cooling augmentation in rectangular channel using two inclined baffles, Int. J. Heat Fluid Flow 2005, 26, 223–232.

[13] Chang S.W. T.-M. Liou, M.H. Lu, Heat transfer of rectangular narrow channel with two opposite scale-roughened walls, Int. J. Heat Mass Transfer 2005, 48, 3921–3931.

[14] Chang S.W., T.-M. Liou, K.F. Chiang, G.F. Hong, Heat transfer and pressure drop in rectangular channel with compound roughness of V-shaped ribs and deepened scales, International Journal of Heat and Mass Transfer 2008, 51, 457–468.

[15] Lee D.H., Dong-Ho Rhee, Kyung Min Kim, Hyung Hee Cho, Hee Koo Moon, Detailed measurement of heat/mass transfers with continuous and multiple V-shaped ribs in rectangular channel, Energy 2009, 34, 1770–1778.
[16] Zhou G., Qiuling Ye, Experimental investigations of thermal and flow characteristics of curved trapezoidal winglet type vortex generators, Applied Thermal Engineering 2012, 37, 241-248.
[17] Pawar S. S., Dr. D. A. Hindolia, J. L. Bhagoria, Enhancement of heat transfer coefficient using Diamond shaped roughness on the absorber plate of solar air heater., International Journal of Engineering Research and Applications 2013, 3(2), 968-974.
[18] Chamoli S., A Taguchi approach for optimization of flow and geometrical parameters in a rectangular channel roughened with V down perforated baffles. Case Studies in Thermal Engineering 2015, 5, 59–69.
[19] Akcayogluand A. and C. Nazli, "Thermal enhancement of triangular fins based on spanwise distance of vortex generators," Proc IMechE Part C: J Mechanical Eng. Science 2016, 1-13.
[20] Alam T., Man-Hoe Kim, "Heat transfer enhancement in solar air heater duct with conical protrusion roughness ribs", Applied Thermal Engineering 2017, 11, 1-37.
[21] Yadav A. D., V. M. Kirplani, Review of Heat Transfer Augmentation within a Plate Heat Exchanger By Different Shapes Of Ribs. International J. of Scientific Eng. & Technology 2013, 2(5), 347-350.
[22] Gawande V.B., A.S.Dhoble, D.B.Zodpe, Effect of roughness geometries on heat transfer enhancement in solar thermal systems-A review. Rene. & Sust. Energy Reviews 2014, 32, 347–378.
[23] Maradiya C., Jeetendra Vadher and Ramesh Agarwal,The heat transfer enhancement techniques and their Thermal Performance Factor, Beni-Suef Univ. J. of Basic & Applied Sciences 2017, 1–21.
[24] Alam T., Man-Hoe Kim, A comprehensive review on single phase heat transfer enhancement techniques in heat exchanger applications. Rene. & Sustainable Energy Reviews 2018, 81, 813–839.
[25] Dittus F.W., L.M.K. Boelter, Univ. of California, Berkeley, CA, Pub. in Engineering 1930, 2, 443 .
[26] Han, J. C. Heat Transfer and Friction in Channels with Two Opposite Rib-Roughened Walls, ASME Journal of Heat Transfer 1984, 106, 774-781.
[27] Prasad BN, Saini JS. Effect of artificial roughness on heat transfer and friction factor in a solar air heater. Sol Energy 1988, 41, 555–60.
[28] Maa T., Qiu-wang, WangMinZeng, Yi-tung Chen, YangLiu, Vijaisr Nagarajan. Study on heat transfer and pressure drop performances of ribbed channel in the High temperature heat exchanger. Applied Energy 2012, 99, 393–401.
[29] Fouladi F., P. Henshaw, D.S.-K. Ting and Steve Ray, "Flat plate convection heat transfer enhancement via a square rib", Int. Journal of Heat and Mass Transfer 2017, 104, 1202–1216.
[30] Yang W., Shulin Xue, Yihong He and Wei Li, "Experimental study on the heat transfer characteristics of high blockage ribs channel", Exp. Thermal and Fluid Science 2017, 83, 248–259.
[31] Dhanawade K. H., Sunnapwar V. K. and Dhanawade H. S., Thermal Analysis of Square and Circular Perforated Fin Arrays by Forced Convection, International Journal of Current Engineering and Technology 2014, Special Issue-2, 109-114.
[32] Latif M. Jiji, Heat Convection, First Edition Springer-Verlag Berlin Heidelberg 2006.
[33] Holman J.P.," Heat Transfer", 6th Edition, McGraw-Hill Book Co. Singapore, 1986.
[34] Yunus A.Çengel, John M. Cimbala FLUID Mechanics: Fundamentals and Applications, Third Edition McGraw-Hill, 2014.
[35] Versteeg, H.K.; Malalasekera, W. An Introduction to Computational Fluid Dynamics the Finite Volume Method, Pearson Education Lmited, 2nd Edition, 2007.
[36] ANSYS CFX Reference Guide. Release 14.0, ANSYS, Inc. Nov 2011.

